

---

# Electron transport through molecules in the Kondo regime: the role of molecular vibrations

J. Mravlje<sup>1</sup> and A. Ramšak<sup>2,1</sup>

<sup>1</sup> Jožef Stefan Institute, Ljubljana, Slovenia, [jerne.j.mravlje@ijs.si](mailto:jerne.j.mravlje@ijs.si)

<sup>2</sup> Faculty of Mathematics and Physics, University of Ljubljana, Slovenia

**Abstract.** We discuss the electronic transport through molecules in the Kondo regime. We concentrate here on the influence of molecular vibrations. Two types of vibrations are investigated: (i) the breathing internal molecular modes, where the coupling occurs between the molecular deformation and the charge density, and (ii) the oscillations of molecule between the contacts, where the displacement affects the tunneling. The system is described by models which are solved numerically using Schönhammer-Gunnarsson's projection operators and Wilson's numerical renormalization group methods.

Case (i) is considered within the Anderson-Holstein model. Here the influence of the phonons is mainly to suppress the repulsion between the electrons at the molecular orbital. Case (ii) is described by a two-channel Anderson model with phonon-assisted hybridization. In both cases, the coupling to electrons softens the vibrational mode and in the strong coupling regime makes the displacement unstable to perturbations that break the symmetry of the confining potential. For instance, in case (ii) when the frequency of oscillations decreases below the magnitude of perturbation breaking the left-right symmetry, the molecule will be abruptly attracted to one of the electrodes. In this regime, the Kondo temperature increases but the conductance through the molecule is suppressed.

## 1.1 INTRODUCTION

The fast pace of the computer industry is mainly driven by the miniaturization of elements in microprocessors. The ultimate limit of the miniaturization is to control the current through individual molecules and it is remarkable that transistors based on single molecules bridging metallic electrodes have already been produced and their current-voltage characteristics have been measured [1–4]. Such molecular junctions are produced using mechanical breaking or electromigration techniques which currently do not allow for scaling up to larger circuits, but they already provide information on the electron transport on the nanoscale that could be essential to the circuitry of tomorrow [5].

Moreover, because the transmission through a molecule is sensitive to its immediate electro-chemical (and also magnetic) environment such devices

could work as molecular sensors. For instance, the binding of guest species to a single host molecule bridging two electrodes has already been discerned in conductance measurements [6]. The studies of conductance could thus enable recognition of single molecules and thereby realize the ultimate limit of analytical chemistry.

In certain regimes the molecular junctions exhibit the Kondo effect [1, 7–9]: the anomalous behavior of conductance due to the increased scattering rate driven by the residual spin (i.e., the quantum impurity) localized at the molecular orbital. The molecular transistors thus provide the nanoscopic realization of quantum impurity models and can be used thus also as a laboratory to investigate many-particle physics, for instance the quantum phase transitions [10].

The transport through molecules is affected by molecular vibrations (MV). The molecular internal vibrational modes and oscillations of molecules with respect to the electrodes explain the side-peaks observed in the non-linear conductance [1, 8, 9, 11]. In this article we are interested in the effects of coupling to the MV at low temperatures and at a small bias (i.e. in the Kondo regime) and their signature in the dependence of the conductance on the gate-voltage.

We consider two different types of molecular vibrations. (i) In the case of breathing molecular modes, i.e., when the MV couple to the electron density, the electron-electron repulsion is effectively diminished and the electron effective mass is enhanced. (ii) When the molecule itself oscillates between the contacts, i.e., the MV modulate the tunneling, the effective repulsion is unmodified but the asymmetrical part of the modulation introduces the charge fluctuations in the odd conduction channel, which leads to the competition between odd and even channel that can result (albeit with some artificial fine-tuning of the models, as we discuss) in the ground state with the non-Fermi liquid 2 channel Kondo fixed point.

Although the influence of the MV on the electrons differs profoundly in these two cases, the back-action of electrons to molecular vibrations is universal. The coupling to electrons tends to soften the molecular modes (diminish their effective frequencies). This softening is related to the increased charge-susceptibility in case (i) or increased susceptibility to breaking of inversion symmetry in case (ii). The result is a suppressed conductance with simultaneous increase of the Kondo temperature.

This contribution provides an overview of our work on quantum impurity models coupled to phonons [12–15]. Because of lack of space we here develop only the main ideas and refer the reader to these articles and the references therein. For background on the Anderson-Holstein model we specifically refer also to [16–18] and for the work on the oscillating molecules we refer also to [19, 20].

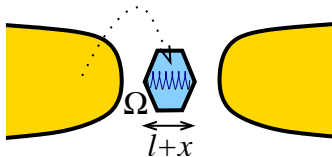


Fig. 1.1. Transport through a molecule with a breathing mode.

## 1.2 Coupling of vibration to charge: Anderson-Holstein model

Consider a molecule with a breathing mode, trapped between two electrodes as depicted schematically on Fig. 1.1. Assuming that a single molecular orbital is relevant for the electron transport (experimentally this assumption is supported by wide inter-orbital energy spacings [8]), the system can be described by the Anderson-Holstein Hamiltonian,

$$H = \sum_{k\alpha} \epsilon_k n_{k\alpha} + \sum_{k\alpha\sigma} \left( V_{k\alpha} c_{k\alpha\sigma}^\dagger d_\sigma + h.c. \right) + \epsilon n + U n_\uparrow n_\downarrow + M(n-1)x + \Omega a^\dagger a \quad (1.1)$$

describing bands of noninteracting electrons in the left ( $\alpha = L$ ) and right ( $\alpha = R$ ) electrodes, with energies  $\epsilon_k$ ,  $n_{k\alpha} = n_{k\alpha\uparrow} + n_{k\alpha\downarrow}$ , which are counted by  $n_{k\alpha\sigma} = c_{k\alpha\sigma}^\dagger c_{k\alpha\sigma}$ . Likewise  $n = n_\uparrow + n_\downarrow$  with  $n_\sigma = d_\sigma^\dagger d_\sigma$  counts the electrons at the molecular orbital with the single-electron energy denoted by  $\epsilon$ ;  $c_{k\sigma}, d_\sigma$  are the electron annihilation and  $c_{k\sigma}^\dagger, d_\sigma^\dagger$  the electron creation operators. The tunneling matrix element between  $k$ -state in the electrode  $\alpha$  and the molecular orbital is given by  $V_{k\alpha}$ . The electrons in the electrodes are assumed noninteracting, the electron repulsion between electrons at the molecular orbital is  $U$ . The charge on the molecular orbital couples to the displacement of the phonon mode  $x = a + a^\dagger$  [ $a^{(\dagger)}$  is the phonon annihilation (creation) operator] via a Holstein coupling of strength  $M$ , while the frequency of the internal vibrational mode of isolated molecule is  $\Omega$ .

Assuming (for simplicity) that the system is inversion symmetric (meaning that the tunneling to the left is equal to the tunneling to the right electrode,  $V_{kL} = V_{kR}$ ) it is convenient to define operators in the electrodes which are even/odd upon inversion

$$c_{e,o} = \frac{1}{\sqrt{2}} (c_L \pm c_R). \quad (1.2)$$

By rewriting the Hamiltonian in the new basis, likewise, the coupling to even channel is given by  $V_e = (1/\sqrt{2})(V_L + V_R)$  and the coupling to the odd channel vanishes  $V_o = (1/\sqrt{2})(V_L - V_R) = 0$ . It is thus sufficient to retain only the even operators explicitly and describe the system by a single channel Anderson-Holstein model.

$$H = \sum_k \epsilon_k n_{ke} + V \sum_\sigma (f_\sigma^\dagger d_\sigma + h.c.) + \epsilon n + U n_\uparrow n_\downarrow + M(n-1)x + \Omega a^\dagger a, \quad (1.3)$$

where  $f_\sigma$  is the linear combination of the conduction electrons to which the molecular orbital (i.e., the impurity) couples directly,

$$f_\sigma = \left( \sum_k V_{ke} c_{ke\sigma} \right) / \left( \sum_k |V_{ke}|^2 \right)^{1/2} = (1/\sqrt{N}) \sum_k c_{ke\sigma}. \quad (1.4)$$

### 1.2.1 Analytical considerations

A convenient starting point for the analysis of the model is to perform the unitary displaced oscillator transformation. One obtains:

$$\begin{aligned} H' &= e^{\frac{M}{\Omega}(a-a^\dagger)(n-1)} H e^{-\frac{M}{\Omega}(a-a^\dagger)(n-1)} = \\ &= \epsilon_{\text{eff}} n + U_{\text{eff}} n_\uparrow n_\downarrow + V \left[ \sum_\sigma f_\sigma^\dagger d'_\sigma + h.c. \right] + \sum_k \epsilon_k n_k + \Omega a^\dagger a, \end{aligned} \quad (1.5)$$

where

$$d' = e^{-\frac{M}{\Omega}(a-a^\dagger)} d; \quad U_{\text{eff}} = U - 2M^2/\Omega; \quad \epsilon_{\text{eff}} = \epsilon + M^2/\Omega. \quad (1.6)$$

The transformed Hamiltonian  $H'$  is of the same form as  $H$ , but with a reduced repulsion  $U_{\text{eff}}$ . The coupling to the phonons is hidden in the transformed operator  $d'$ . The transformed boson operators read,

$$a' = a - \frac{M}{\Omega}(n-1). \quad (1.7)$$

The displacement is shifted depending on the occupancy of the molecular orbital

$$x' = x - 2M(n-1)/\Omega. \quad (1.8)$$

There is an interesting large-frequency limit  $M/\Omega \rightarrow 0$ , but  $M^2/\Omega$  finite, where the coupling to phonons is entirely described in terms of the effective parameters of the model.

The same result follows from considering the EP interaction perturbatively [16]. A pair of EP vertices and a phonon propagator can be formally substituted by a frequency-dependent point electron-electron interaction vertex. The influence of the phonon mode is then retained in the frequency dependence of the interaction

$$U(\omega) = U + M^2 D_0(\omega) = U - \frac{2M^2\Omega}{\Omega^2 - \omega^2}, \quad (1.9)$$

because  $D_0(\omega) = 2\Omega/(\omega^2 - \Omega^2)$ . At low frequencies the interaction is screened due to the formation of bipolarons  $U(\omega \rightarrow 0) = U_{\text{eff}}$ , at high frequencies the bare interaction is recovered. If  $\Omega$  is large, then the low-energy behavior is given entirely by the Anderson model with  $U_{\text{eff}}$ . Note that effective repulsion can become negative; that provides the motivation for studies in the  $U < 0$  regime.

### 1.2.2 Numerical results

The results presented here are discussed in more detail in [12]. The results for repulsive  $U$  as a function of gate voltage  $\epsilon + U/2$  are presented in Fig. 1.2 with full lines. On the top panel the conductance, in the middle panel the average charge and on the bottom panel the fluctuations of charge are plotted. In the Kondo regime, where the average charge  $\langle n \rangle \sim 1$ , the conductance is enhanced towards the unitary limit  $G \rightarrow G_0$ . The maximal conductance is given by the quantum of conductance  $G_0 = 2e^2/h$  ( $h$  is the Planck's constant,  $e$  the electron charge) and corresponds to the unitary transmission [21, 22]. Actually, the average charge and conductance are related by the Friedel sum rule

$$G = G_0 \sin^2 \frac{\pi}{2} n. \quad (1.10)$$

The Friedel sum rule in this form holds for single-impurity parity symmetric models. The generalization to non-symmetric case is possible [13].

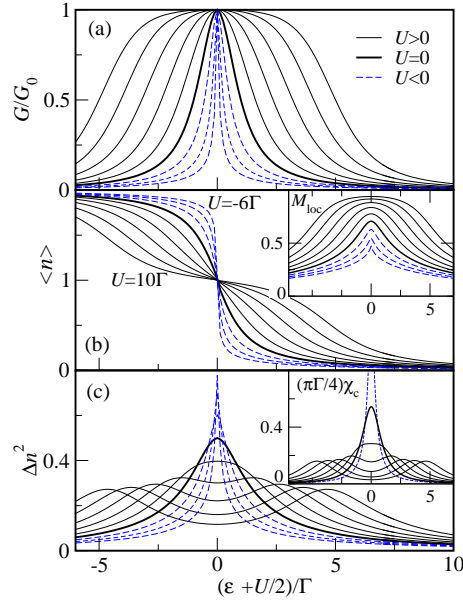


**Fig. 1.2.** (a) Conductance for the Anderson model with  $-6\Gamma \leq U \leq 10\Gamma$  in increments of  $2\Gamma$  (full lines for  $U > 0$ , dashed lines for  $U < 0$  and a thicker full line for  $U = 0$ ). (b) Local occupancy  $n$  and local moment  $M_{\text{loc}}$  (inset). (c) Charge fluctuations  $\Delta n^2 = 2n - n^2 - M_{\text{loc}}^2$ . Inset: renormalized charge susceptibility  $(\pi\Gamma/4)\chi_c$ .

The fingerprint of the Kondo physics is also the appearance of the local moment  $M_{\text{loc}} = \langle (n_{\uparrow} - n_{\downarrow})^2 \rangle^{1/2}$ , presented in the inset of Fig. 1.2(b) and

the suppression of the charge fluctuations  $\Delta n^2 = \langle (n - \langle n \rangle)^2 \rangle$ , Fig. 1.2(c). In the inset the corresponding charge susceptibility,  $\chi_c = -\partial n / \partial \epsilon$  is given. In agreement with the fluctuation-dissipation theorem, the charge fluctuations are similar to the charge susceptibility,  $\Delta n^2 \sim (\pi\Gamma/4)\chi_c$ . Strictly,  $\langle n^2 \rangle$  is given with the integral of the imaginary part of the dynamic charge susceptibility,  $\chi_c''(\omega)$ , therefore the relation to static  $\chi_c$  is only qualitative.

In Fig. 1.2(a) the conductance for various  $U < 0$  is presented with dashed lines. The first observation is a narrowing of the conductance curve and the corresponding enhanced charge fluctuations [Fig. 1.2(c)], consistent with a sharp transition in the local occupation and a suppression of the local moment, Fig. 1.2(b). For increasing  $|U|$ , the charge susceptibility diverges and overshoots the charge fluctuations.

For general values of parameters, i.e., for moderate  $\Omega$ , the problem with EP coupling cannot be mapped onto the Anderson model. However, the behavior is still to the largest extent determined by  $U_{\text{eff}}$ , and similar to the above discussed results, Fig. 1.2. For example, the result of the Schrieffer-Wolff transformation is now an anisotropic Kondo model [23], where the anisotropy stems from the fact that the phonon displacement couples only to the  $z$ -component of the isospin  $T_z$ .

In addition to the renormalization of  $U$  now also the hybridization is renormalized as shown on Fig. 1.3, where the results for bare  $U = 5\Gamma$  case are compared to the  $U = 10\Gamma, U_{\text{eff}} = 5\Gamma$  case for  $\Omega = 10\Gamma$ ,  $\Omega = \Gamma$  and  $\Omega = \Gamma/100$ . The smaller the  $\Omega$ , the sharper the jump in the conductance corresponding to an enhanced effective mass due to the larger effect of  $e^{-\frac{M}{\Omega}(a-a^\dagger)}$ .

The results for very soft phonons  $\Omega = \Gamma/100$  can also be understood in an alternative manner. In the Kondo regime the conductance is close to the bare Anderson model result with  $U = 10\Gamma$ . In the mixed valence regime the curve is much steeper, due to a strong renormalization [24] of the hopping. In the empty-orbital regime the conductance approaches the result obtained with a doubly reduced electron-electron interaction

$$U_{\text{eff}} = U - \frac{4M^2}{\Omega}, \quad (1.11)$$

which can be understood as follows. First the oscillator displacement is shifted,  $x \rightarrow \tilde{x} + 2\lambda$  thus the Hamiltonian is transformed into

$$\tilde{H} = (\epsilon + 2\lambda M)n + \tilde{x}[M(n-1) + \Omega\lambda] + \Omega\tilde{a}^\dagger\tilde{a} + \dots, \quad (1.12)$$

where  $\lambda = -M(n-1)/\Omega$ , with vanishing transformed displacement. This Hamiltonian can be solved with trial wave functions with no phonons. The renormalized local energies are then  $\epsilon + 2M^2/\Omega$ ,  $\epsilon$ , and  $\epsilon - 2M^2/\Omega$  for  $n = 0, 1, 2$ , respectively. The shifts of  $\epsilon$  where  $n = 0, 2$  in turn correspond to reduced  $\tilde{U} = U - 4M^2/\Omega$  and to  $\tilde{U} = U$  for  $n = 1$ .

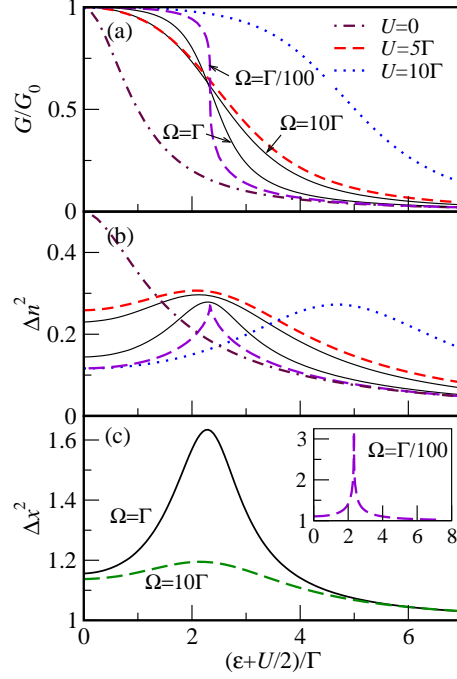


**Fig. 1.3.** A fixed  $U = 10\Gamma$  and  $U_{\text{eff}} = 5\Gamma$  with for  $\Omega = \Gamma$ ,  $\Omega_2 = 10\Gamma$  and  $\Omega_2 = 10\Gamma$ . Also plotted are the results for a bare Anderson model with  $U = 10\Gamma$ ,  $U = 5\Gamma$  and  $U = 0$  (dotted, short-dashed and dashed-dotted, respectively). (a) Conductance, (b) occupation fluctuations and (c) deformation fluctuations. In the inset, the deformation fluctuations for a softer mode are shown.

### 1.2.3 Softening of the phonon mode

Phase transitions are ubiquitously related to the instability of the symmetry restoring modes. In ferroelectrics, for instance, the para $\rightarrow$ ferro phase transition will occur when the unstable phonon is frozen-in to one of the equivalent configurations [25, 26]. As the temperature is tuned towards the transition,  $T \rightarrow T_c$  the related static temperature-dependent susceptibility will diverge,  $\chi(T) = C/(T - T_c)$ . According to the Kramers-Kronig relation

$$\chi(T) = \chi'(0, T) = \frac{2}{\pi} \int_0^\infty \frac{\chi''(\omega', T)}{\omega'} d\omega' \quad (1.13)$$

this will occur when the dissipative imaginary part of the susceptibility  $\chi''(\omega)$  has a peak at low frequencies. As poles of  $\chi''(\omega)$  indicate the normal modes of the system, the frequency of the normal mode  $\omega_0$  should vanish at the transition.

There is a remarkable analogy to this behavior in the strong-coupling regime of the Anderson-Holstein model (although there is no phase transi-

tion; we are dealing with a single degree of freedom here). As shown in the inset of Fig. 1.2(c), the charge susceptibility  $\partial n/\partial\epsilon$  diverges for large  $M$ . The charge-charge correlation function should also increase there according to the fluctuation-dissipation theorem. Due to the Holstein coupling of charge to the displacement it seems plausible that the phonon correlation function should also be influenced. Indeed, in the Anderson-Holstein model the charge-charge and the displacement-displacement correlation functions are directly related

$$D(\omega) = D_0(\omega) + M^2 D_0(\omega) \ll (n-1), (n-1) \gg_\omega D_0(\omega), \quad (1.14)$$

as can easily be proved by considering the equation of motion. The phonon propagator must thus develop a low frequency component. The phonon mode is softened as  $M$  grows large. On Fig. 1.4 the NRG results for imaginary part of the phonon propagator

$$\mathcal{A}(\omega) = -\frac{1}{\pi} \text{Im} \ll x, x \gg_\omega = -\frac{1}{\pi} \text{Im} \int_0^\infty (-i) \langle [x(t), x(0)] \rangle e^{i\omega t} dt \quad (1.15)$$

are plotted. The oscillations which occur at frequency  $\Omega$  for the uncoupled

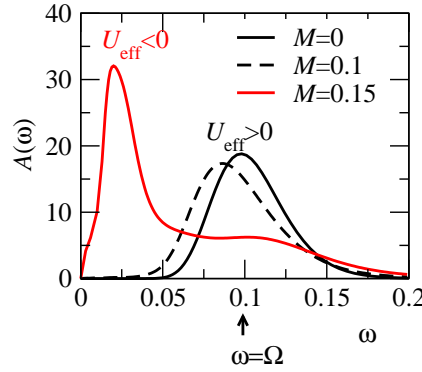


**Fig. 1.4.** The displacement-displacement spectral function for  $\Omega/\Gamma = 5$ ,  $U/\Gamma = 15$ ,  $M/\Gamma = 0, 5, 7.5$ .

oscillator become with increasing electron phonon coupling softer and their characteristic frequency diminishes. The spectral functions are broadened on the logarithmic scale as in [15].

The softening can also be related to the change in the shape of the effective potential the oscillator experiences due to the coupling to the electrons. The effective potential can be extracted using the SG method as explained in [15]. The results are shown in Fig. 1.5. We see that when the sign of the effective repulsion is changed, the oscillator potential will evolve to a double well form. The displacements of large magnitude (corresponding to displaced oscillator



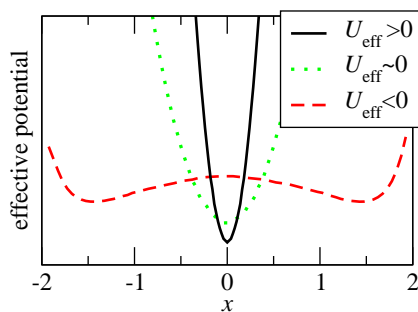


**Fig. 1.5.** Effective potential for  $U/\Gamma = 7.5$ ,  $\Omega/\Gamma = 2.5$ , and  $M/\Omega = 1.15, 1.25, 1.35$ .

transformation for states of double and zero occupancy) will be preferred. The low frequency component of the propagator corresponds to slow fluctuations of the oscillator between the degenerate minima of the effective potential, the high-frequency component corresponds to fast oscillations within the wells.

### 1.3 Oscillations with respect to the leads

We now turn to the case where the molecule oscillates between the electrodes. We model the system with the Hamiltonian, Eq. (1.1) for  $M = 0$ , but with phonon-assisted hopping induced by the displacement dependent tunneling matrix elements  $V_{k\alpha} \rightarrow V_{k\alpha}(x)$ , as schematically presented on Fig. 1.6.

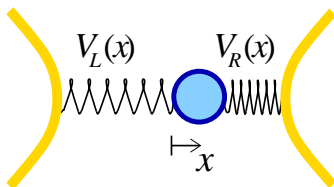


**Fig. 1.6.** (Color online) Schematic plot of the model device.

The full Hamiltonian thus reads,

$$H = \sum_{k\alpha} \epsilon_k n_{k\alpha} + \sum_{k\sigma} \left[ V_{k\alpha}(x) c_{k\alpha\sigma}^\dagger d_\sigma + h.c. \right] + \epsilon n + U n_\uparrow n_\downarrow + \Omega a^\dagger a. \quad (1.16)$$

From now on, we are here interested in the particle-hole symmetric point  $\epsilon = -U/2$ , where the molecule is on average singly occupied. We use  $U = 15\Gamma$ . Other details of calculation can be found in [15]. Again, it is practical to define

even and odd combinations of states in the electrodes, and in this basis the tunneling part of the Hamiltonian reads,

$$V_e(x)\hat{v}_e + V_o(x)\hat{v}_o \quad (1.17)$$

where

$$V_{e,o}(x) = \frac{V_L(x) \pm V_R(x)}{\sqrt{2}}, \quad (1.18)$$

modulate the tunneling to even and odd channels. Hybridization operators are  $\hat{v}_\alpha = f_{\sigma\alpha}^\dagger d_\sigma + h.c.$  for  $\alpha = e, o$ , respectively, where  $f_e$  is the even combination of electrode orbitals and  $f_o$  is the odd combination of electrode orbitals. Note that

$$|V_e(x)| > |V_o(x)| \quad (1.19)$$

if  $V_{L,R}(x)$  are both positive or both negative for all  $x$ .

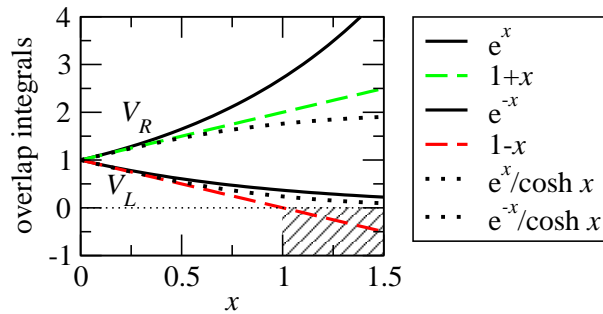


**Fig. 1.7.** (Color online) Various forms of the tunneling-modulation. The unphysical regime of LM where the tunneling starts to increase with increasing distance to the electrode is indicated by dashing.

### 1.3.1 Two-channel Kondo model

The odd channel is coupled to the molecule only due to the asymmetric modulation of tunneling. For example, in the linear approximation  $V_{L,R}(x) = V(1 \mp gx)$  the even channel is coupled to the molecule directly and the odd channel is coupled to the molecule via a term proportional to  $gx$ . Unlike in the Anderson-Holstein model, the attempts to eliminate the coupling to phonons using a variant of Lang-Firsov transformation fail. Note that the coupling to phonons as considered in this Section does not affect the effective repulsion but it affects the hybridization and therefore the Kondo temperature can be enhanced [15].

As a consequence of the coupling the molecular orbital to two channels the low-energy behavior is that of the two-channel Kondo (2CK) model [19, 27].

The screening of the spin occurs in the channel with the larger coupling constant. If the couplings match, an overscreened, i.e., a genuine 2CK problem with a non-Fermi liquid behaviour results. For a linearized model to be introduced below such a fixed point has indeed been found at an isolated value of the electron-phonon coupling with simulations based on numerical renormalization group [14, 15, 28].

### 1.3.2 Overlap integrals

The calculations are performed using several functional forms of  $V_\alpha(x)$  depicted in Fig. 1.7. In a realistic experimental situation the tunneling between the molecule and the tip of an electrode will be saturated at small distances and it will progressively decrease with increasing distance of the molecule from the electrode. The precise functional dependence of overlap integrals will in general depend on details of the molecule and the tips of the electrodes, but the overall behavior should be as shown in Fig. 1.7(a) with dotted line.

#### Linearized modulation

The simplest form of overlap integrals is obtained by the expansion to lowest order in displacement resulting in linear modulation (LM)

$$V_{L,R}(x) = V [1 \mp (gx + \zeta)]. \quad (1.20)$$

The tunneling matrix element, constant  $V$  for  $g = 0$ , is linearly modulated by displacement for  $g > 0$ . We assume the system is almost inversion symmetric. A small  $\zeta \geq 0$  is the magnitude of the symmetry breaking perturbation. In the symmetrized basis the overlap integrals take on the following form

$$V_e = \sqrt{2}V, \quad V_o = \sqrt{2}V(gx + \zeta). \quad (1.21)$$

Note that Eq. (1.21) does not satisfy the requirement Eq. (1.19) for  $gx > 1 - \zeta$ , because the overlap to the left electrode becomes negative and its absolute value starts to increase with increasing  $x$  (dashed region in Fig. 1.7).

#### Regularized modulation

A more realistic approximation to overlap integrals is the exponential dependence on displacement but it breaks down at small distance to the electrodes as discussed exhaustively in [15]. The modulation should therefore at large displacements be regularized and for the rest of this paper we use

$$V_{L,R}(x) = V [\exp(\mp gx) / \cosh(gx) \mp \zeta], \quad (1.22)$$

or in the symmetrized basis

$$V_e = \sqrt{2}V, \quad V_o = \sqrt{2}V [\tanh(gx) + \zeta]. \quad (1.23)$$

The inequality Eq. (1.19) is satisfied (the 2CK fixed point is thus inaccessible) and the normalization with the cosh function ensures that the hybridization saturates at small distances to the electrodes.

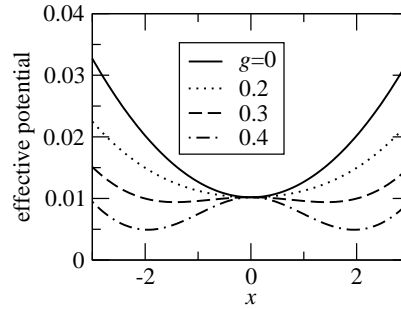


**Fig. 1.8.** Semi-classical estimate of effective oscillator potential for tanh modulation. Parameters  $\Omega = 0.01$ ,  $\Gamma = 0.02$  are in units of  $D$  (half-width of the band).

### 1.3.3 Effective potential

At  $U = 0$  and replacing operators  $a, x$  by real valued quantities, the model Eq. 1.16 is solvable exactly and the energy of the ground state as a function of  $x$  provides the estimate of the effective oscillator potential. This simple estimate agrees qualitatively with the results of more elaborate methods [15]. We plot the results on Fig. 1.8.

Initially harmonic potential softens with increasing  $g$  and at a certain point a double well potential develops. The softening thus occurs similarly as in the case of Anderson-Holstein model but here it is related to the dynamical breaking of inversion symmetry [19]. Due to the softening, the instability towards perturbations breaking the symmetry (degeneracy between the two minima of the double-well potential) can be expected. On the mean field level [13], the instability is indeed seen as a tendency towards an asymmetric ground state with large average  $x$  in systems *with* inversion symmetry.

## 1.4 Numerical results

The development of the double well potential induces fluctuations of displacement and its influence can also be seen in the NRG results of static quantities shown on Fig. 1.9 for  $U = 0.3$ ,  $\Gamma = 0.02$ ,  $\Omega = 0.01$ . In these results an inversion symmetry breaking perturbation of strength  $\zeta = 0.01$  is included.

The average displacement presented on Fig. 1.9(a) increases as the electron-phonon coupling is increased. The fluctuations of displacement initially increase then they diminish, as the oscillator gets trapped in the lower of the two-well potential (also this behavior is discussed in more detail in [15]). At large electron-phonon coupling also the average displacement starts to diminish. This happens because for tanh-form of the hybridization for large  $g$  the hybridization is maximal already for small displacements and therefore the system can minimize the elastic energy without cost in the kinetic energy.

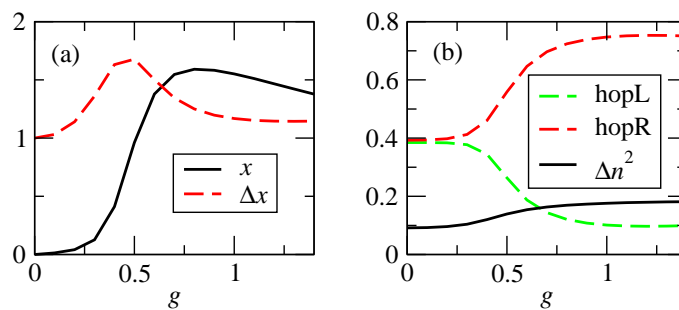


**Fig. 1.9.** (Color online) (a) Displacement and displacement fluctuations. (b) Average hopping to left and right; fluctuations of charge.

On Fig. 1.9(b) also the electronic expectation values are shown. At large  $g$ , the molecule is near the right lead as signified by increased hopping to the right. The total hybridization and, correspondingly, the charge fluctuations are also increased there. The Kondo temperature is increased, but the conductance is suppressed due to the asymmetric configuration [15].

The softening of the potential is seen also in the displacement spectral function shown on Fig. 1.10. Similar to the behavior discussed in the previous chapter, the frequency of vibration diminishes with increasing  $g$ , because the confining potential is softened. At large  $g$  the molecule is trapped to the lower of the two wells, the oscillations between the two-wells become unfavourable and the spectral weight is again transferred to high frequencies corresponding to oscillations within the lower of the two wells.

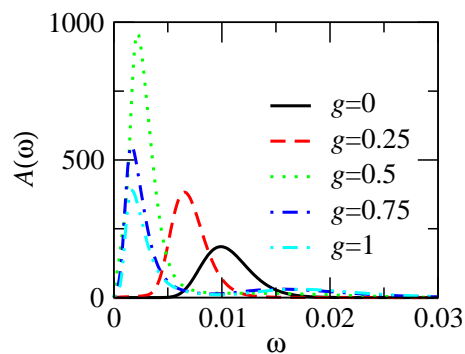


**Fig. 1.10.** (Color online) Displacement spectral functions for parameters as in Fig. 1.9.

## 1.5 Conclusion

We invoked Anderson model coupled to phonons to describe the transport through the molecule coupled to molecular vibrations. While the influence the MV exhibit on electron depends on the details of the coupling, the coupling to electrons tends to soften the MV. In the strong coupling regime of the Anderson-Holstein model ( $U_{\text{eff}} < 0$ ), a perturbation of the orbital energy drives the system from the particle-hole symmetric point characterized with zero average displacement of the oscillator. Likewise, in the Anderson model with asymmetrically modulated hybridization, a perturbation of the left-right symmetry results in a state with large average displacement (the molecule is attracted to one of the electrodes).

### 1.5.1 Discussion

In measurements of conductance through molecular junctions the side-peaks pertaining to the excitation/annihilation of vibrational quanta are clearly discerned at a finite bias. The influence of phonons in the equilibrium at a small bias is less investigated, because it does not appear to affect the measured conductance significantly. Why is this so?

The answer is that systems with electron-phonon (EP) coupling to internal molecular modes can usually be reformulated in a manner that refers to the EP coupling only by a redefinition (renormalization) of the original (bare) parameters, which themselves are not, unfortunately, known to start with. For instance, such a parameter is the repulsion, which is effectively diminished due to the influence of the EP coupling. But because the repulsion is diminished already for a decoupled molecule any attempt to discern the effects of the Holstein phonon by comparing to the data for isolated molecules will likely prove in vain.

If one was interested in discriminating the effects of the coupling to phonons nevertheless, a convenient quantity to look at would be the frequency dependence of the local charge susceptibility. In the regime of reduced repulsion due to the EP coupling, the charge would be susceptible to the oscillations of gate voltage only below the phonon frequency. In order to investigate this experimentally, one would need to be able to measure the time dependence of molecular charge. While this currently seems a formidable task, we note that in quantum dots (QDs) the time-resolved measurements of charge using quantum-point contacts have already been demonstrated, e.g. in [29].

In near future, there is more hope to discern the effects of the EP coupling to the contacts. However, even qualitative effects – such as the breaking of the particle-hole (PH) symmetry, which occurs when the breathing modes couple to the electron charge and modulate the tunneling at the same time – can be dominated by non-perfectly symmetric contacts. But still, measuring the linear conductance to a better precision and comparing the data for rigid molecules to the data for softer molecules could unravel the influence of the

breathing oscillations and the type of their coupling to the electron transport in the equilibrium.

The case of molecules oscillating between the electrodes is a bit different. One particular effect of the EP coupling is obvious. Imagine a break junction with a single molecule bridging the two contacts. In principle, one can slowly increase the tension between the contacts, until they separate. Any tiny perturbation of the parity will choose a contact to which the bridging molecule will be attracted. This is precisely the physics analyzed here: the tension pulls the contacts apart and the separation sets the modulation of tunneling by induced displacement of the molecule. With increasing tension also the modulation increases. The potential confining the molecule to the center is softened, and instantly, the molecule is attracted to one of the contacts.

One might argue that the idea is rather to get as close to the breaking point to observe the onset of the non-Fermi liquid (NFL) fixed point. But because NFL fixed point corresponds to the case when the molecule fluctuates between far left *and* far right, the conductance is zero as is also if the molecule is far left *or* far right. It is worth calculating the temperature dependence of conductance and hope for some anomalies due to the NFL formation energy scale (for a very recent work in this direction see [28]), but we anticipate that it will be difficult to distinguish the results from these corresponding to the displacement of the molecule towards one of the contacts only.

On the other hand, one could observe the effects of the phonon-mode softening directly in nanoelectromechanical suspended cantilevers. Consider the setup, depicted in Fig. 1.11. The cantilever (blue) oscillates between the aux-

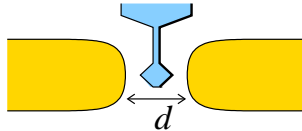


**Fig. 1.11.** Scheme of the proposed device.

iliary contacts (gold). The frequency of oscillations can be detected independently, e.g. by a quantum-point contact shifted perpendicularly with respect to the plane defined by the cantilever and the contacts [30]. We predict that the frequency of oscillations will decrease when the distance between the contacts  $d$  is diminished provided that the device will operate in the regime of coherent tunneling.

It would be interesting also to investigate the softening by suppressing it with the magnetic field. For magnetic fields above the Kondo temperature the spin at the orbital is frozen. According to the Pauli principle the charge fluctuations and the transport of electrons are blocked. Simultaneously, also the related kinetic energy gain vanishes and the softening is suppressed [31].

## References

1. J. Park, A.N. Pasupathy, J. I. Goldsmith, C. Chang, Y. Yaish, J.R. Petta, M. Rinkoski, J.P. Sethna, H.D. Abrunas, P.L. McEuen, D.C. Ralph, *Nature* **417**, 722 (2002)
2. A. Nitzan, M.A. Ratner, *Science* **300**, 1384 (2003)
3. N.J. Tao, *Nature Nanotech.* **1**, 173 (2006)
4. M. Galperin, M.A. Ratner, A. Nitzan, *J. Phys.: Condens. Matter.* **19**, 103201 (2007)
5. D. Natelson, *Phys. World* **22**, 26 (2009)
6. X. Xiao, B. Xu, N. Tao, *Angew. Chem. Int. Edn* **43**, 6148 (2004)
7. A.C. Hewson, *The Kondo Problem to Heavy Fermions* (Cambridge University Press, 1993)
8. L.H. Yu, D. Natelson, *Nano Lett.* **4**, 79 (2004)
9. A.N. Pasupathy, J. Park, C. Chang, A.V. Soldatov, S. Lebedkin, R.C. Bialczak, J.E. Grose, L.A.K. Donev, J.P. Sethna, D.C. Ralph, P.L. McEuen, *Nano Lett.* **5**, 203 (2005)
10. N. Roch, S. Florens, V. Bouchiat, W. Werndorfer, F. Balestro, *Nature* **453**, 633 (2008)
11. N.B. Zhitenev, H. Meng, Z. Bao, *Phys. Rev. Lett* **88**, 226801 (2002)
12. J. Mravlje, A. Ramšak, T. Rejec, *Phys. Rev. B* **72**, 121403(R) (2005)
13. J. Mravlje, A. Ramšak, T. Rejec, *Phys. Rev. B* **74**(20), 205320 (2006)
14. J. Mravlje, A. Ramšak, R. Žitko, *Physica B* **403**, 1484 (2008)
15. J. Mravlje, A. Ramšak, *Phys. Rev. B* **78**, 235416 (2008)
16. A.C. Hewson, D. Meyer, *J. Phys: Condens. Matter* **14**(3), 427 (2002)
17. P.S. Cornaglia, H. Ness, D.R. Grempel, *Phys. Rev. Lett.* **93**(14), 147201 (2004)
18. P.S. Cornaglia, D.R. Grempel, H. Ness, *Phys. Rev. B* **71**(7), 075320 (2005)
19. C.A. Balseiro, P.S. Cornaglia, D.R. Grempel, *Phys. Rev. B* **74**(23), 235409 (2006)
20. P. Lucignano, G.E. Santoro, M. Fabrizio, E. Tosatti, *Phys. Rev. B* **78**, 155418 (2008)
21. S. Datta, *Electronic transport in Mesoscopic Systems* (Cambridge University Press, 1995)
22. H. van Houten, C.W.J. Beenakker, *Phys. Today* **49**, 22 (1996)
23. T.A. Costi, *Phys. Rev. Lett.* **80**(5), 1038 (1998)
24. K. Schönhammer, O. Gunnarsson, *Phys. Rev. B* **30**(6), 3141 (1984)
25. R. Blinc, B. Žekš, *Soft Modes in Ferroelectrics and Antiferroelectrics* (North-Holland – American Elsevier, 1974)
26. P.W. Anderson, *Basic notions of condensed matter physics* (The Benjamin/Cummings Publishing Company, Inc., 1984)
27. P. Nozières, A. Blandin, *J. Physique (France)* **41**, 193 (1980)
28. L.G.G.V.D. da Silva, E. Dagotto, *Phys. Rev. B* **79**, 155302 (2009)
29. J.R. Petta, A.C. Johnson, J.M. Taylor, E.A. Laird, A. Yacoby, M.D. Lukin, C.M. Marcus, M.P. Hanson, A.C. Gossard, *Science* **309**(5744), 2180 (2005)
30. M. Poggio, M.P. Jura, C.L. Degen, M.A. Topinka, H.J. Mamin, D. Goldhabed-Gordon, D. Rugar, *Nature Phys.* **4** (2008)
31. M. Fabrizio and E. Tossatti, internal communication (2009)